scientific reports

Check for updates

OPEN

Dynamics and conditions for inhibitory synaptic current to induce bursting and spreading depolarization in pyramidal neurons

Hongtao Hua[1,2], Huaguang Gu[2]✉, Kaihua Ma[3], Yanbing Jia[4] & Liang Wu[1]

Enhanced activity of inhibitory neurons, which is often used to suppress behaviors of pyramidal neurons to treat brain diseases, whereas can enhance spiking to a mixed-mode bursting (MMB) in recent experiments on migraine and seizure. The MMB contains a phase with high level of membrane potential/extracellular potassium concentration ($[K^+]_o$), which can propagate to form spreading depolarization (SD) wave. Different from the common view that the MMB/SD is often induced by enhanced positive effect or $[K^+]_o$, in the present paper, dynamics and conditions for the uncommon MMB/SD evoked by enhanced inhibitory synaptic current are obtained in a theoretical model. Firstly, in addition to the well-known positive threshold across which the common MMB is induced by positive effect, a spiking pyramidal neuron exhibits a novel negative threshold with a low level of $[K^+]_o$ for the MMB. A long and strong inhibitory stimulation suppresses the spiking to silence phase via a saddle-node bifurcation on an invariant circle at first and then run across the negative threshold, triggering positive feedback to enhance membrane potential and $[K^+]_o$ to levels high enough, then resulting in the uncommon MMB. Secondly, in a coupling model, enhanced inhibitory effect for enhanced spiking activity of interneuron and conductance of inhibitory synapse, and enhanced spiking activity of pyramidal neuron, are favorable for the uncommon MMB. Then, reducing these activities or parameters present potential measures to prevent the MMB. Finally, in network model, the uncommon MMB of a pyramidal neuron can induce SD wave. The results present a novel theoretical explanation to the uncommon MMB/SD, counterintuitive function of the inhibitory interneuron, and potential measures to treat the diseases.

Keywords Spreading depolarization, Bursting, Bifurcation, Negative threshold, Inhibitory interneuron, Migraine

The electrical activities of the nervous systems modulated by the excitatory and inhibitory effects exhibit complex nonlinear dynamics, which are involved in various functions[1–3]. For example, the enhanced firing activities of the pyramidal neurons, which are often induced by the reduced inhibitory effect of the interneurons, are related to various brain diseases containing the seizure[4–6]. Then, enhancing activities of the inhibitory neurons to suppress activities of pyramidal neurons is an important measure to treat the diseases[7–10]. However, the enhanced inhibitory effects of interneurons can induce enhanced activities of pyramidal neurons in many studies[11–13]. A representative is post-inhibitory rebound (PIR) spiking, i.e., inhibitory synaptic current of interneuron can induce spiking from resting state of pyramidal neuron, along with seizure, presenting a novel etiology of seizure[14–16] and a counterintuitive effect of inhibitory modulation. In theory, the PIR phenomenon can be well understood with a "negative" threshold of membrane potential, different from the well-known "positive" threshold[17–20]. The membrane potential for the "positive" threshold is higher than that of the resting state, whereas for the "negative" threshold is lower than that of the resting state. During an inhibitory stimulation, the decreased membrane

[1]School of Mathematics and Science, Henan Institute of Science and Technology, Xinxiang 453003, China. [2]School of Aerospace Engineering and Applied Mechanics, Tongji University, Shanghai 200092, China. [3]School of Mathematics and Physics, Jiangsu University of Technology, Changzhou 213001, China. [4]School of Mathematics and Statistics, Henan University of Science and Technology, Luoyang 471000, China. ✉email: guhuaguang@tongji.edu.cn

can pass through the "negative" threshold to trigger the spiking. The "negative" threshold is related to Hopf bifurcation at first[17] and then to the saddle-node bifurcation on an invariant cycle (SNIC)[18,19].

In addition to the PIR spiking, another representative is observed in recent experiments on type III familial hemiplegic migraine (FHM)[21,22] and a special case of seizure[23–26]. Enhanced activity of the inhibitory interneuron, which is enhanced by gene (*SCN1A*) mutation of the sodium channel or photogenetic stimulation, cannot suppress but enhance the spiking of the pyramidal neurons to a mixed-mode bursting (MMB). The MMB exhibits a phase with high level of membrane potential/extracellular potassium concentration ($[K^+]_o$), which can propagate on the cerebral cortex to form spreading depolarization (SD) wave[21,22,27,28]. Such MMB induced by enhanced activity of interneuron is called uncommon MMB bursting in the present paper, distinguished with the common MMB often induced by enhanced excitatory effect or $[K^+]_o$[29–32]. For the common MMB evoked from spiking of pyramidal neuron, positive/excitatory effect or $[K^+]_o$ is elevated to a level high enough to trigger positive feedback between the elevations of membrane potential (excitability) and $[K^+]_o$, forming the burst phase and the depolarization block phase with high level of membrane potential/$[K^+]_o$. The key characteristic of the MMB is that $[K^+]_o$ manifests nearly "all-or none" pulse, similar to action potential. In some theoretical studies[24–26], enhanced spiking activity of interneuron is suggested to enhance $[K^+]_o$ through releases of K^+ to extracellular volume, then, the uncommon MMB reported in Refs[21,22] is explained in theoretical models with ion concentrations such as $[K^+]_o$ considered as variables[24–26]. Then, questions arise. If the release of K^+ of interneuron is ignored, can the inhibitory synaptic current induce the uncommon MMB? If the answer is yes, many questions underlying the uncommon MMB arise. For example, the conditions of interneuron, pyramidal neuron, and inhibitory synapse for the uncommon MMB, the dynamical mechanism for the uncommon MMB, and the SD wave for the uncommon MMB in the network, remain unclear.

In the present paper, at first, the uncommon MMB is reproduced in a pyramidal neuron and a coupling model composed of a pyramidal neuron and an interneuron with inhibitory synaptic current, which presents a novel view on the uncommon MMB. Then, the SNIC bifurcation and "negative" threshold for the uncommon MMB are obtained, different from the "positive" threshold, which presents theoretical explanations to the uncommon MMB. The threshold is for $[K^+]_o$ instead of membrane potential. During the inhibitory stimulation, the behavior runs across the "negative" threshold to trigger positive feedback to induce the depolarization block phase, which presents deep understanding to the uncommon MMB. Furthermore, the conditions to evoke or eliminate the uncommon MMB are obtained, presenting potential measures to modulate brain diseases. Enhanced inhibitory effect for enhanced spiking activity of interneuron or conductance of inhibitory synapse, and enhanced spiking activity of pyramidal neuron, are favorable for the uncommon MMB. Then, reducing these activities or parameters presents potential measures to prevent the MMB. Finally, in a network model, the uncommon MMB of a single pyramidal neuron can induce SD, presenting a novel view on the SD.

Results

Dynamics of a single pyramidal neuron

Bifurcations from resting state to spiking

The bifurcations of V_e of pyramidal neuron are shown in Fig. 1a. With increasing the depolarization current J_e, the resting state (left solid black curve, a stable node, $J_e < 1.40$ μA) changes to bursting in a narrow range (cyan, $1.40 < J_e \leq 1.64$ μA) via a saddle-node bifurcation on an invariant circle (SNIC, $J_e \approx 1.40$ μA), to spiking (green, $1.64 < J_e \leq 5.61$ μA), to common mixed-mode bursting (MMB) (yellow, $5.61 < J_e \leq 7.87$ μA), to small oscillation in a narrow range (gray, $7.87 < J_e < 8.26$ μA), and to depolarization block (right solid black curve, a stable focus) via a Hopf bifurcation (H, $J_e \approx 8.26$ μA). In Fig. 1a, the red curves denote the peak and valley values of V_e, and dashed black curve represents the unstable fixed points.

The stable equilibrium points before SNIC are depicted in plane ($[K^+]_o$, $[Na^+]_i$), as shown in Fig. 1b. The decrease of J_e induces spiking changed to these stable equilibrium points via the SNIC, which plays an important role in recognizing the uncommon MMB induced by inhibitory stimulation. The equilibrium points for $J_e = 1.18$ μA is labeled as P0, and the SNIC point correspond to $J_e \approx 1.40$ μA, which are used to explain the uncommon MMB.

The spiking behaviors for $J_e = 2$ and 4 μA are illustrated in Fig. 1c, d, respectively, with frequency increased from 3.6 to 12.6 Hz, where the dark blue and red denote V_e and $[K^+]_o$, respectively. $[K^+]_o$ of the spiking is lower than 7 mM. For $J_e = 6$ μA, the MMB exhibits a depolarization block phase with high level of V_e and $[K^+]_o$ (~25.94 mM) following many spikes, as shown in Fig. 1e. Compared Fig. 1c–e, $[K^+]_o$ for spiking exhibits subthreshold oscillations, whereas $[K^+]_o$ for MMB manifests nearly "all-or-none" pulse, which is the key characteristic of the MMB. The MMB is induced by the increase of J_e, i.e., a common MMB. Bursting pattern and small oscillation are not shown here (not the focus of the present paper).

A "positive" threshold of $[K^+]_o$ for common MMB induced by elevation of $[K^+]_o$

As illustrated in Fig. 2a, for the spiking at $J_e = 4$ μA (upper panel, green), a pulse of $[K^+]_o$ (lower panel, $\Delta [K^+]_o = 5.6$ mM) applied to a point A can evoke a common MMB (upper panel, blue). The $[K^+]_o$ pulse

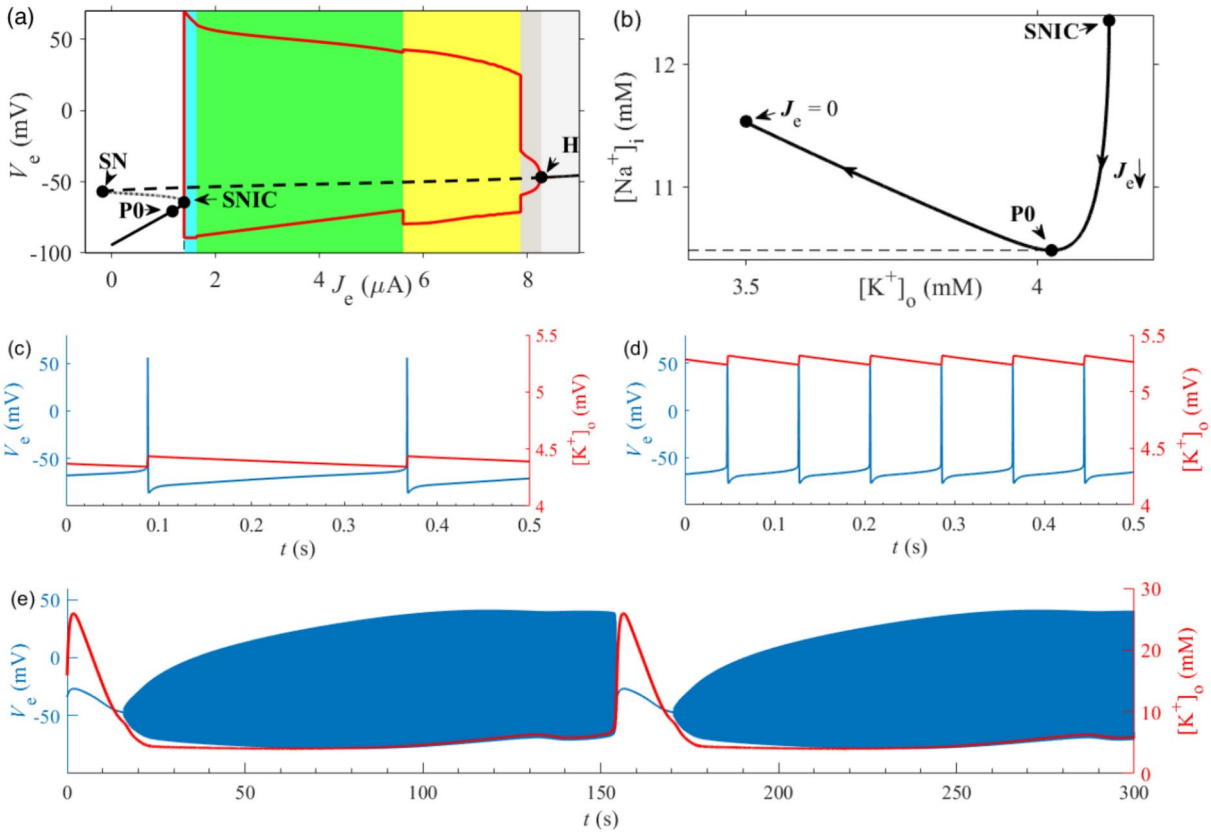

Fig. 1. Dynamical behaviors of the isolated pyramidal neuron. (**a**) Bifurcations with respect to J_e for membrane potential V_e; (**b**) The stable equilibrium points before SNIC in plane ($[K^+]_o$, $[Na^+]_o$); Spiking for $J_e = 2$ μA (**c**) and for $J_e = 4$ μA (**d**); (**e**) Common MMB for $J_e = 6$ μA (2 cycles); Dark blue represents membrane potential (V_e) and red denotes $[K^+]_o$.

terminates at the point B1 (0.001 ms after point A). Points A and B1 correspond to the onset and termination phases of the stimulation, respectively. Phase between C1 and D1 is the depolarization block phase. There are small oscillations around point D1. Around point E1 is the recovery phase of the spiking. The enlargement of the burst before the depolarization block phase is illustrated in Fig. 2b, showing positive feedback between the increase of the spiking frequency/membrane potential level and the accumulation/elevation of $[K^+]_o$[33–35].

The threshold for the MMB induced from the spiking at $J_e = 4$ μA is obtained, as shown by the dashed and dotted curves in the plane ($[K^+]_o$, $[Na^+]_i$) in Fig. 2c. The green and blank areas divided by the threshold curve are the spiking and MMB regions, respectively. The "positive" threshold is represented by the dashed black curve, with $[K^+]_o$ higher than that of the initial spiking (point A). For the common MMB, the projection of the phase trajectory (solid curve) after the point A run across the "positive" threshold. In addition, as shown in Fig. 2d, the "positive" threshold in ($[K^+]_o$, $[Na^+]_i$, V_e) is shown by the gray surface, which is nearly independent of V_e. Then, the threshold for the MMB is mainly for $[K^+]_o$ instead of V_e, which is very different from the negative threshold for membrane potential to induce the PIR phenomenon[17–19].

In addition to the "positive" threshold (dashed black curve), it should be noticed that there is the "negative" threshold, denoted by dotted black curve, which has $[K^+]_o$ lower than that of the initial spiking (point A). The "negative" threshold in plane ($[K^+]_o$, $[Na^+]_i$) resembles that for membrane potential in plane (V, n) (n is activation variable of potassium channel) to induce the PIR phenomenon[17–19]. Obviously, the "positive" and "negative" thresholds are divided by the level of $[K^+]_o$ of spiking (point A). Inhibitory or negative stimulation can cause the phase trajectory passed through the "negative" threshold, forming the uncommon MMB, which are addressed in the following paragraphs. In addition, the threshold is dependent of other variables such as $[Na^+]_i$, which is not the focus of the present paper, since $[K^+]_o$ is the dominant factor in many studies[21,22,24–26].

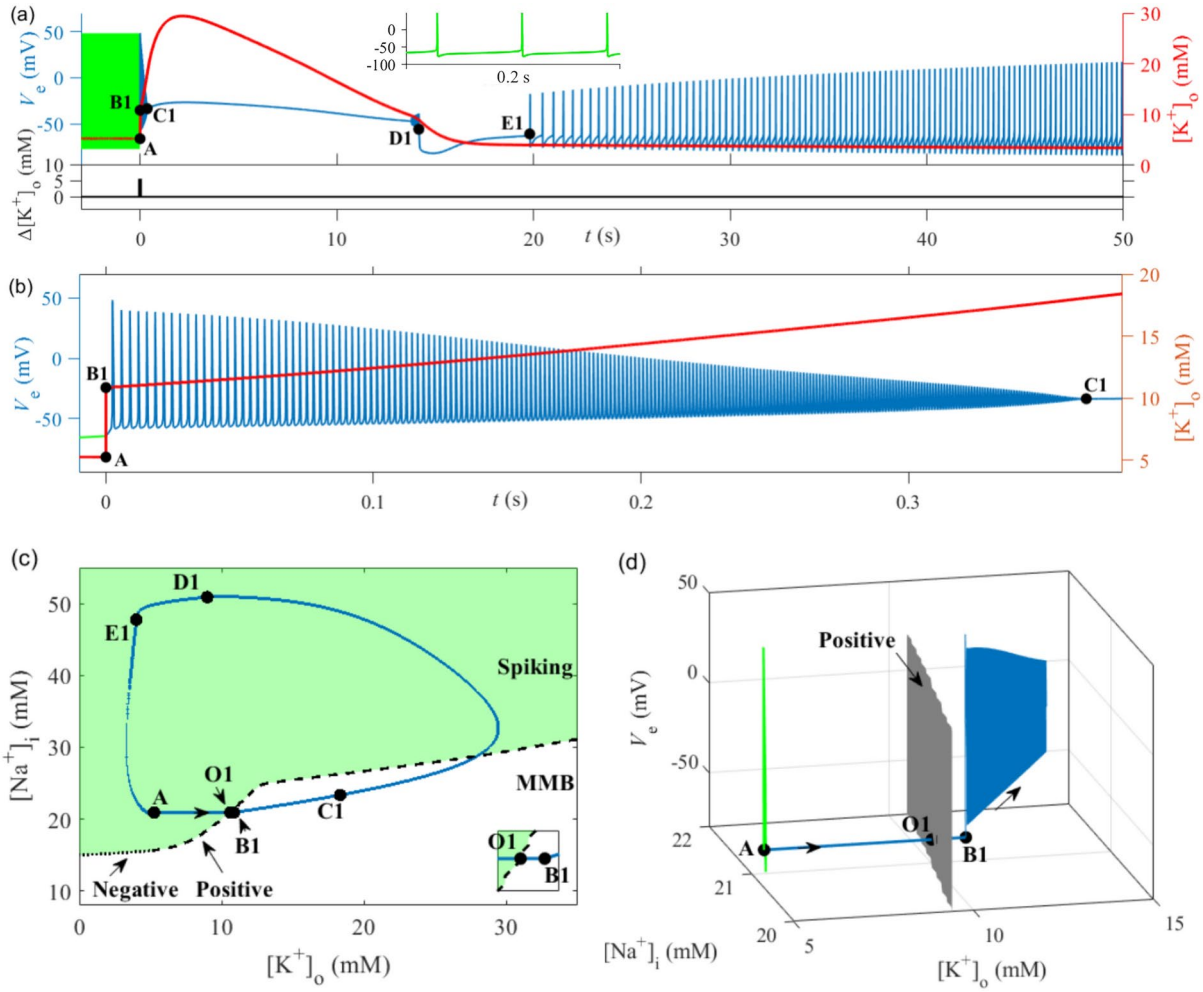

Fig. 2. The common MMB and the "positive" threshold. (**a**) MMB (blue, upper panel) induced from the spiking (green, upper panel) by the elevation of $[K^+]_o$ pulse (lower panel). Red represents $[K^+]_o$; (**b**) Enlargement of the burst phase in panel (**a**); (**c**) Phase trajectory (blue solid), "positive" threshold (dashed black curve), and "negative" threshold curve (dotted black curve). Point O1 is the intersection point where the trajectory crosses the positive threshold curve. The inset is a magnified view near the point O1; (**d**) The part around the point O1 in panel (**c**) plotted in space ($[K^+]_o$, $[Na^+]_i$, V_e). Point O1 is the point at which the trajectory intersects the positive threshold surface (gray).

Strong and long inhibitory current induce uncommon MMB via passage through the "negative" threshold and SNIC bifurcation

The results for negative square current stimulations with long duration (1200 s) are depicted in Fig. 3a, with four stimulation strengths considered as representatives. Strong stimulation strengths, such as $I_{app} = -2.62$, -2.82, and -3.39 μA, can induce spiking for $J_e = 4$ μA (point A) changed to stable equilibrium P2, P0, and P1, respectively, which locate on the stable equilibrium curve (solid black, same as Fig. 1b) and in the MMB region. However, weak stimulation, such as $I_{app} = -2.2$ μA, cannot induce spiking changed to stable equilibrium, but still spiking (point B2). The border between the strong and weak stimulations is that $I_{app} = 1.4 - 4 = -2.6$ μA, where 1.4 μA corresponds to J_e value of the SNIC bifurcation. Stimulations stronger and weaker than -2.6 μA correspond to strong and weak stimulations, respectively. It is via the SNIC bifurcation that the strong negative square current can induce spiking changed to stable equilibrium. Interestingly, the stable equilibriums locate in the MMB region which is lower than the "negative" threshold (dotted curve), whereas the point B2 in the spiking region upper to the "negative" threshold. Then, after termination of the stimulation, uncommon MMB appears for strong stimulation with duration 1200 s, as shown in Fig. 3c ($I_{app} = -2.62$ μA), whereas not uncommon MMB but spiking for weak stimulation for $I_{app} = -2.2$ μA, as shown in Fig. 3d. The inset in Fig. 3c shows an enlarged view of the burst and depolarization block phases.

For the strong stimulation strength ($I_{app} = -2.82$ μA), stimulation duration is also an important factor to induce the uncommon bursting, as shown in Fig. 3b, with three stimulation durations considered. From

point A to P0 corresponds to stimulation duration 1200 s, same as the dark blue in Fig. 3a. As stimulation duration is shortened to 200 s, the behavior runs to point B3, which locates on the trajectory from point A to P0. Although not reaching the stable equilibrium point P0, the trajectory from point A to B3 still runs across the "negative" threshold. Then, uncommon MMB appears following the point B3, as shown in Fig. 3e. As stimulation duration is shortened to 30 s, the behavior reaches to point B4 locating on the trajectory from point A to P0. Unfortunately, the trajectory from point A to B4 does not pass through the "negative" threshold. Then, following the point B4 is spiking instead of uncommon MMB, as shown in Fig. 3f. Combined with Fig. 3c (long and strong stimulation induces uncommon bursting) and Fig. 3d (weak and long stimulation cannot induce uncommon bursting), it can be concluded that only strong and long inhibitory stimulation can induce uncommon MMB in a single neuron. In the following subsection, the uncommon MMB in the coupling model is studied.

The conditions and dynamics for the uncommon MMB in the coupling model

The coupling model is composed of a pyramidal neuron receiving synaptic current of an interneuron (Fig. 10a). The enhancement of activity of interneuron is considered.

Inhibitory interneuron: enhanced firing frequency with increasing g_{Nai} or J_i

With increasing sodium conductance g_{Nai} or depolarization current J_{i} of interneuron, spiking frequency increases (from blue to green to red), as shown in Fig. 4a, exclusive the left black for the resting state. The increase of g_{Nai} corresponds to the overexpression of Na^+ channels of interneurons for type III FHM[21,22]. As illustrated in Fig. 4b with $J_{\mathrm{i}} = 1$ μA, there is a homoclinic orbit bifurcation (Hom, $g_{\mathrm{Nai}} \approx 22.4$ mS/cm^2) between the resting state and spiking as g_{Nai} changes, and the spiking rate increases from ~ 58 Hz for $g_{\mathrm{Nai}} \approx 22.4$ mS/cm^2 with increasing g_{Nai}. As depicted in Fig. 4c with $g_{\mathrm{Nai}} = 35$ mS/cm^2, the resting state changes to spiking through a saddle-node bifurcation on an invariant cycle (SNIC at $J_{\mathrm{i}} \approx 0.1$ μA), and the spiking rate increases from 0 Hz for $J_{\mathrm{i}} \approx 0.1$ μA. The spiking rate for $J_{\mathrm{i}} = 0.97$ μA (labeled as J_{i0}) approximates ~ 58 Hz. The range of spiking rate for g_{Nai} is a part of that for J_{i}. The difference of spiking rate induced by g_{Nai} and J_{i} induces different behaviors for g_{Nai} and J_{i} in the coupling model (Fig. 5). The spiking trains corresponding to the cycles in Fig. 4b and Fig. 4c are shown in Fig. 4d and Fig. 4e, respectively.

Fast instead of slow spiking of pyramidal neuron is favorable for the uncommon MMB

The pyramidal neuron with high frequency spiking ($3 \le J_{\mathrm{e}} \le 5$ μA) are studied, and the behaviors of pyramidal after receiving the inhibitory synaptic current from the interneuron are shown in Fig. 5. The distributions of behaviors in 3-dimensional space ($J_{\mathrm{e}}, g_{\mathrm{GABA}}, J_{\mathrm{i}}$) and ($J_{\mathrm{e}}, g_{\mathrm{GABA}}, g_{\mathrm{Nai}}$) are depicted in Fig. 5a, b, respectively. The range of J_{i} for Fig. 5a corresponds to spiking of interneuron in Fig. 4c, and $J_{\mathrm{i0}} = 0.97$ μA corresponds to spiking rate ~ 58 Hz. The range of g_{Nai} for Fig. 5b corresponds to spiking of interneuron in Fig. 4b, and $g_{\mathrm{Nai}} = 22.4$ mS/cm^2 corresponds to spiking rate ~ 58 Hz. Yellow represents the uncommon MMB, and green, cyan, and light gray denote spiking, bursting, and silence, respectively. Obviously, uncommon MMB (yellow) is evoked from pyramidal neuron with relatively high frequency spiking, i.e., large J_{e}. The uncommon MMB cannot be evoked for the pyramidal neuron with low frequency spiking, i.e., small J_{e}. The behaviors upper to the dashed line in Fig. 5a are similar to those in Fig. 5b.

Fast spiking of interneuron and large conductance of inhibitory synapse are favorable for the uncommon MMB

As shown in Fig. 5, interneuron with high spiking frequency (large J_{i} or g_{Nai}), and strong conductance of inhibitory current (large g_{GABA}), are favorable for the uncommon MMB. The results show that the inhibitory current of the interneuron instead of the release of K^+ of interneuron can also induce the uncommon MMB, which presents a novel mechanism for the uncommon MMB observed in the experiments[21,22]. The uncommon MMB cannot be evoked for low spiking frequency (small J_{i} or small g_{Nai}). To further show the roles of the interneuron and inhibitory synapse, the behaviors of pyramidal neuron in planes ($J_{\mathrm{i}}, g_{\mathrm{GABA}}$) and ($g_{\mathrm{Nai}}, g_{\mathrm{GABA}}$) for $J_{\mathrm{e}} = 4$ μA are illustrated in Fig. 6(a1) and (a2). For the strong inhibitory effect of the interneuron, i.e., large J_{i}, g_{Nai}, and g_{GABA}, the uncommon MMB is induced, as shown by the yellow area. The behavior is still spiking (green) for small J_{i}, g_{Nai}, or small g_{GABA}. Horizontal and vertical dotted lines represent $g_{\mathrm{GABA}} = 1.5$ mS/cm^2 and $J_{\mathrm{i}} = 2$ μA, respectively. The results for $4 < J_{\mathrm{e}} \le 5$ μA are similar (not shown here).

The weak inhibitory synaptic current for small J_{i} plays a suppression role, as shown in top two rows of right column of Fig. 6. For $J_{\mathrm{i}} = 0$ μA, the behavior of the interneuron is resting state (dashed line), as depicted in Fig. 6(b1), the spiking (blue solid line) of pyramidal neuron for $J_{\mathrm{e}} = 4$ μA remains unchanged (~ 12.6 Hz), since the inhibitory current to pyramidal neuron is zero. As J_{i} changes to 0.51 μA, the interneuron exhibits spiking with frequency ~ 33 Hz, as illustrated by dashed blue curve in Fig. 6(b2), which induce inhibitory synaptic current to cause a drop of V_{e} (solid blue curve) to prolong the interspike intervals of spiking (solid blue curve) of pyramidal neuron, resulting in a reduced frequency ~ 8.2 Hz. As J_{i} increases to 4 μA, corresponding to the last circle on the horizontal line in Fig. 6(a1), the uncommon MMB is shown in Fig. 6(b3). The uncommon MMB exhibits four phases: burst (orange), depolarization block (green) with high level of V_{e} and $\left[K^+\right]_{\mathrm{o}}$ (higher than 20 mM), small oscillations (brown), and silence phase with a low V_{e} (blue, between S1 and R1), resembling those of the experiment[21,22]. The enlargement around the burst in Fig. 6(b3) is depicted in Fig. 6(b4). The positive feedback to elevate $\left[K^+\right]_{\mathrm{o}}$ and level of membrane potential/spiking rate to form the uncommon MMB can be found. The results along the three vertical triangles for $J_{\mathrm{i}} = 2$ μA in Fig. 6(a1) show similar dynamics (not shown here).

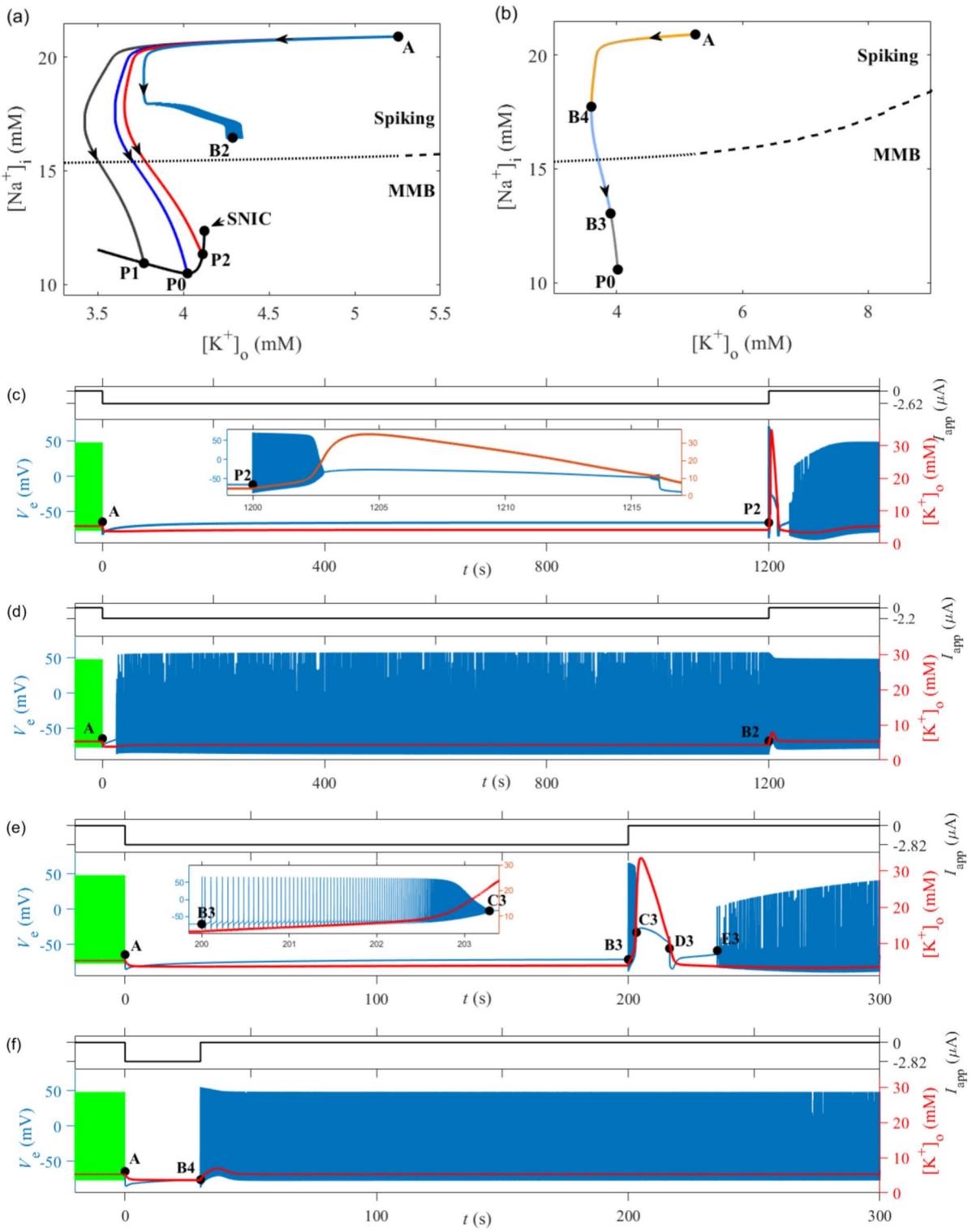

Strong/long inhibitory synaptic current induces uncommon MMB

The reduced spiking shown in Fig. 6(b2) receives a weak inhibitory synaptic current, as depicted in Fig. 7a. The inhibitory current between two spikes of the pyramidal neuron is small and short (exclusive the peak induced by action potential), as shown in the inset panel. The valley value is weaker than –2 μA, and is shorter than 0.2 s. The inhibitory current during the silence of the uncommon MMB depicted in Fig. 6(b3) is long and strong, as shown in Fig. 7c, showing that the inhibitory current with long duration and strong strength can induce the uncommon MMB. The inhibitory current with long duration and strong strength is induced by the high firing frequency of interneuron. For the reduced spiking, the firing rate of interneuron is low, and the gate variable s almost decays to 0 between two action potentials of the interneuron, as illustrated in Fig. 7b. Then, the inhibitory synaptic current is weak. Differentially, for the uncommon MMB, the firing rate of interneuron is high. Then,

◂**Fig. 3**. Strong and long inhibitory stimulation induces uncommon MMB from spiking (green) for $J_e = 4$ μA. (**a**) Phase trajectories for $I_{app} = -2.62$ (red), -2.82 (dark blue), and -3.39 μA (gray) with duration 1200 s, respectively, run across the "negative" threshold (dotted black curve), where for $I_{app} = -2.2$ (light blue) not; (**b**) The phase trajectory from A to P0, B3, and to B4 is induced by $I_{app} = -2.82$ μA with duration 1200 s, 200 s, and 30 s. Membrane potential (light blue) and $[K^+]_o$ (red): (**c**) $I_{app} = -2.62$ μA for 1200 s induces uncommon MMB. The inset shows an enlarged view of the burst and depolarization block phases; (**d**) $I_{app} = -2.2$ μA for 1200 s cannot induce uncommon MMB; (**e**) $I_{app} = -2.82$ μA for 200 s induces uncommon MMB. The inset represents an enlarged view of the burst phase. (**f**) $I_{app} = -2.82$ μA for 30 s cannot induce uncommon MMB. Point A stands for the onset phase of inhibitory stimulation, while points B2, B3, and B4 signify the offset phase of inhibitory stimulation. Between C3 and D3 is the depolarization block phase, and after E3 is the recovery process of spiking.

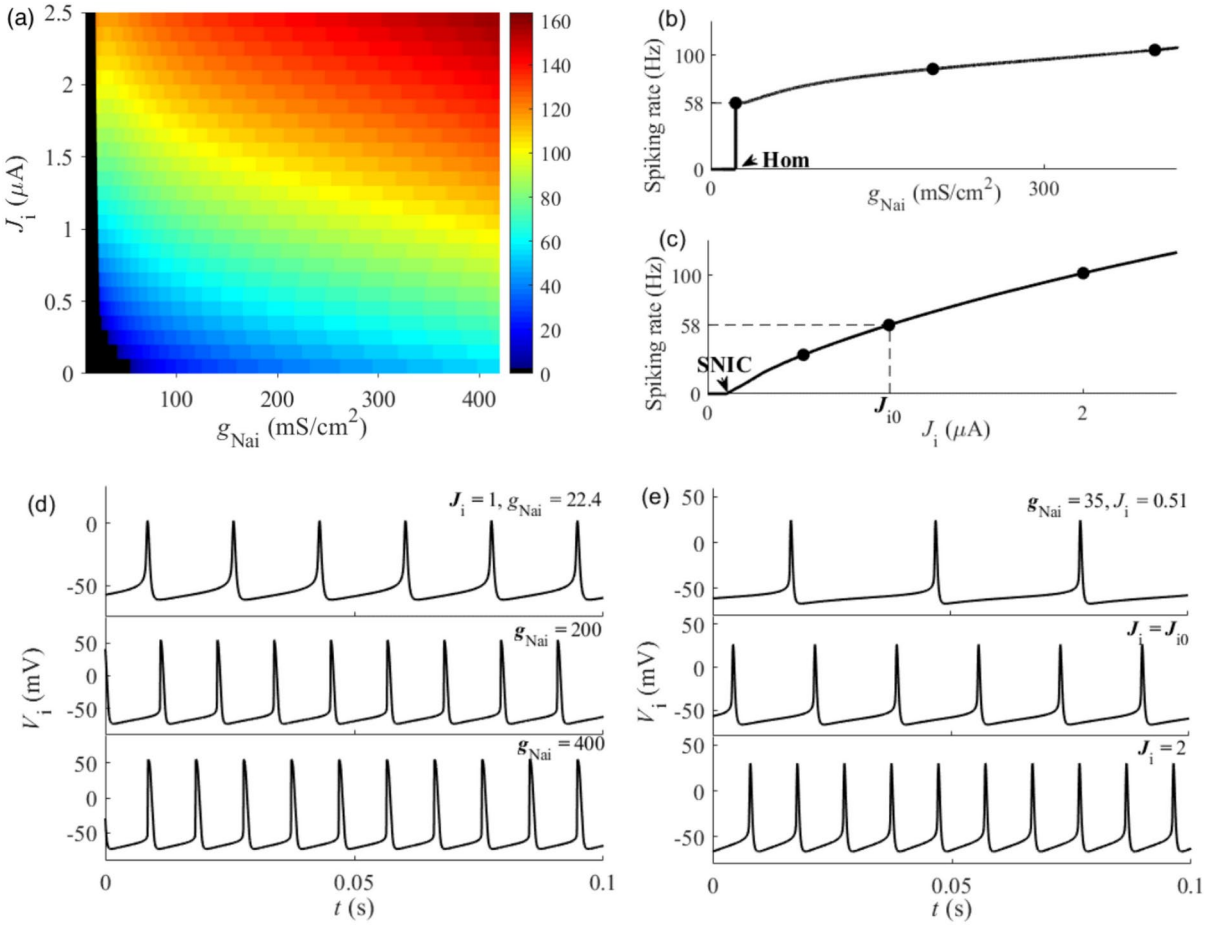

Fig. 4. Enhanced firing activity with increasing g_{Nai} or J_i of the inhibitory interneuron. (**a**) Spiking rate in the plane (g_{Nai}, J_i); (**b**) Changes of spiking rate with increasing g_{Nai} for $J_i = 1$ μA; (**c**) Changes of spiking rate with increasing J_i for $g_{Nai} = 35$ mS/cm^2; (d) Spike trains for different circles of panel (**b**); (**e**) Spike trains for different circles of panel (**c**). Hom and SNIC denote homoclinic orbit bifurcation and saddle-node bifurcation on an invariant circle, respectively.

the gate variable s exhibits fast oscillations and cannot decay to zero (larger than 0.5), as shown in Fig. 7d. Then, the inhibitory current is strong.

"Negative" threshold for the uncommon MMB

The phase trajectory of the uncommon MMB (red) for Fig. 6(b3) can run across the "negative" threshold (dashed black curve) in the plane ($[K^+]_o$, $[Na^+]_i$), as depicted in Fig. 8a. The passage through the "negative" threshold happens in the silence phase between R2 and S2. The trajectory (red) of uncommon MMB for the upper triangle in Fig. 6(a1) passes through the "negative" threshold (dashed black curve), as shown in Fig. 8b. The results show that the uncommon bursting for the coupling model also runs across the "negative" threshold. The spiking corresponding to the left circle and lower triangle of Fig. 6(a1) is shown by the green in Fig. 8a, b,

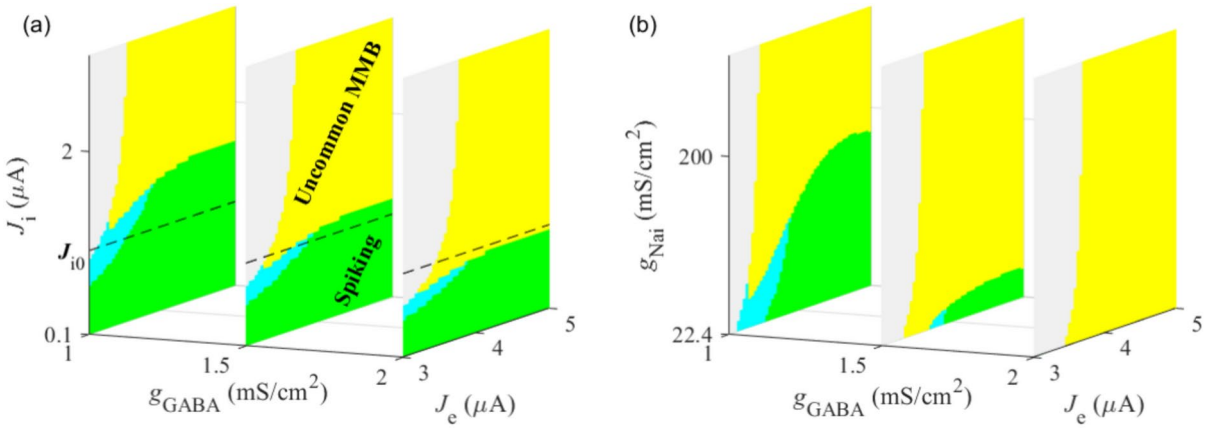

Fig. 5. Distribution of dynamical behaviors of pyramidal neuron. (**a**) On the plane (J_e,J_i) at different g_{GABA} (g_{Nai} = 35 mS/cm^2); (**b**) On the plane (J_e,g_{Nai}) at different g_{GABA} (J_i = 1 μA); Yellow, green, cyan, and light gray denote uncommon MMB, spiking, bursting, and silence, respectively. J_{i0} = 0.97 μA corresponds to spiking rate ~ 58 Hz.

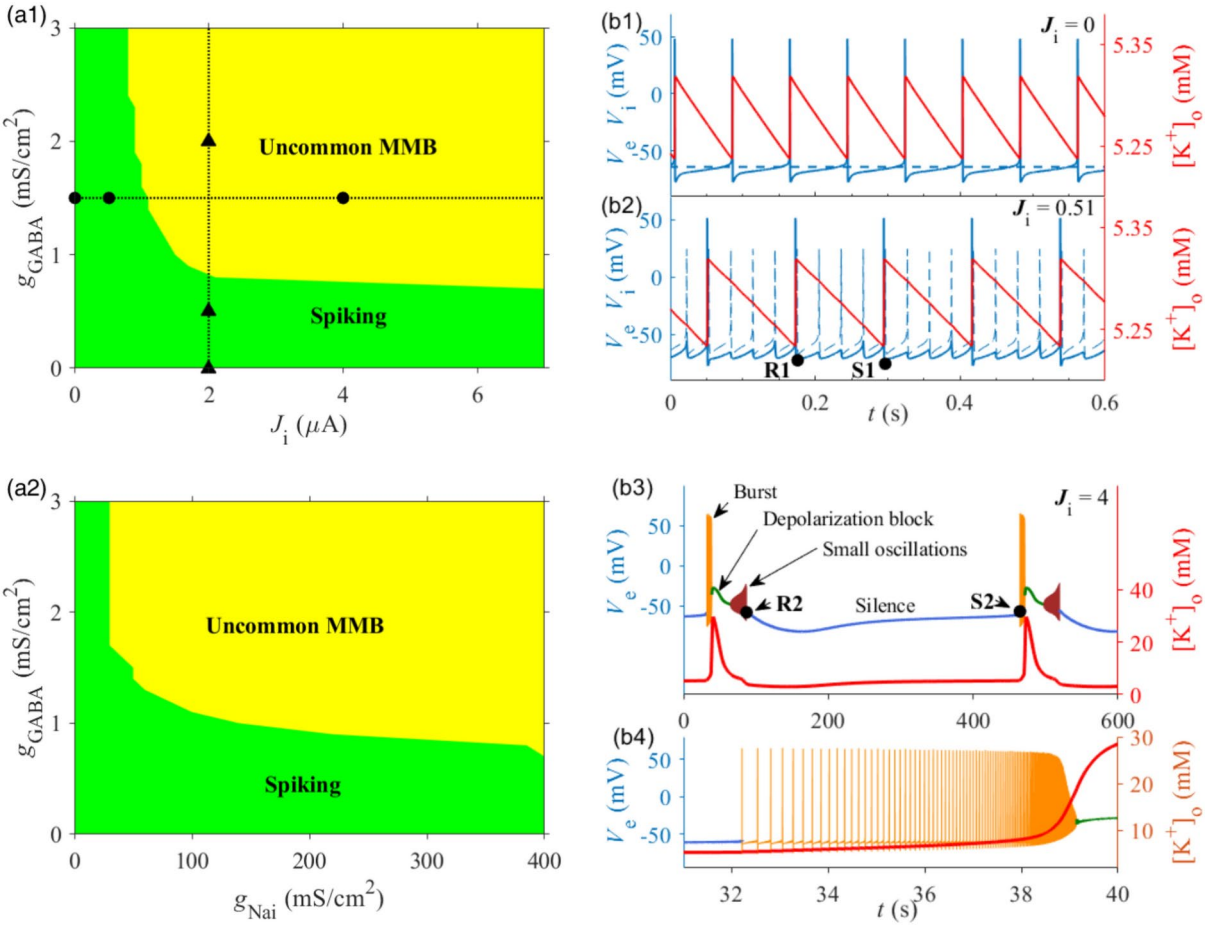

Fig. 6. Spiking (green) and uncommon MMB (yellow) for J_e = 4 μA. (a1) Distribution in the plane (J_i, g_{GABA}) for g_{Nai} = 35 mS/cm^2; The black cycles on the line g_{GABA} = 1.5 mS/cm^2 correspond to J_i = 0, 0.51, and 4 μA, respectively, from left to right; The black triangles on the line J_i = 2 μA correspond to g_{GABA} = 0 , 0.5, and 2 mS/cm^2, respectively, from bottom to top; (a2) Distribution in the plane (g_{Nai}, g_{GABA}) for J_i = 1 μA. Membrane potential and $[K^+]_o$ (red) with g_{GABA} = 1.5 mS/cm^2: (b1) Spiking for J_i = 0 μA; (b2) Reduced spiking for J_i = 0.51 μA; (b3) Uncommon bursting for J_i = 4 μA; (b4) Enlargement of burst before depolarization block phase in panel (b3).

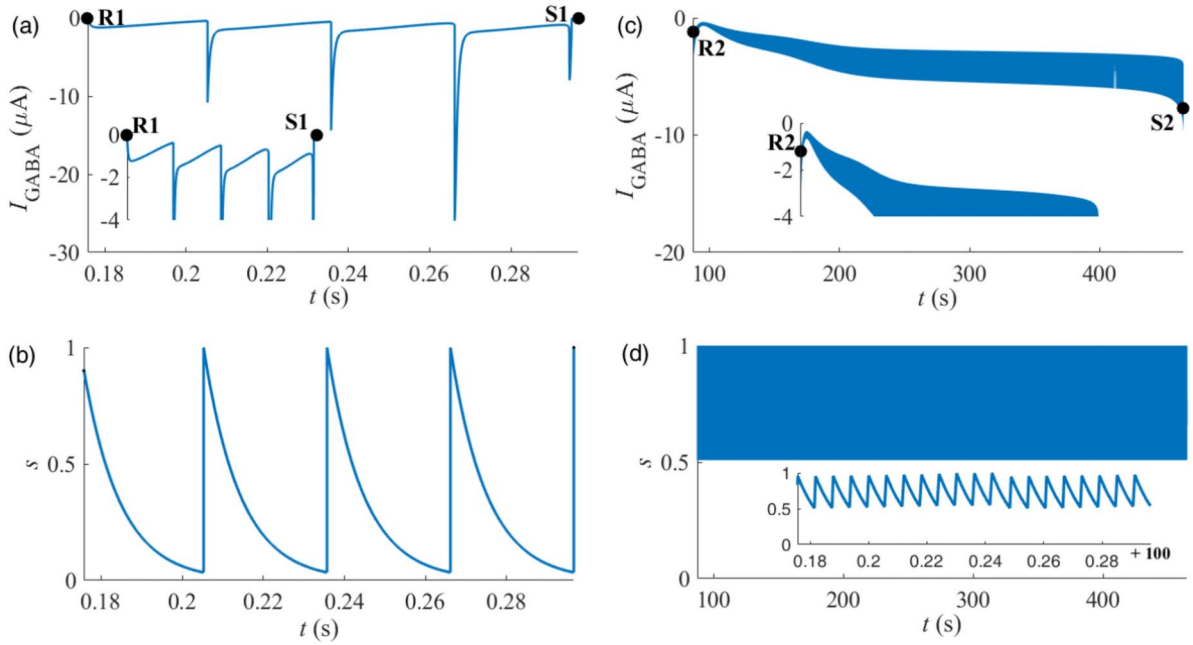

Fig. 7. Inhibitory synaptic current (upper row) and gate variable s (lower row). (**a**) I_{GABA} between two spikes of pyramidal neuron in Fig. 6(b2); (**b**) The gate variable s for panel (**a**); (**c**) I_{GABA} during the silence phase (between R2 and S2) in Fig. 6(b3); (**d**) The gate variable s for panel (**c**).

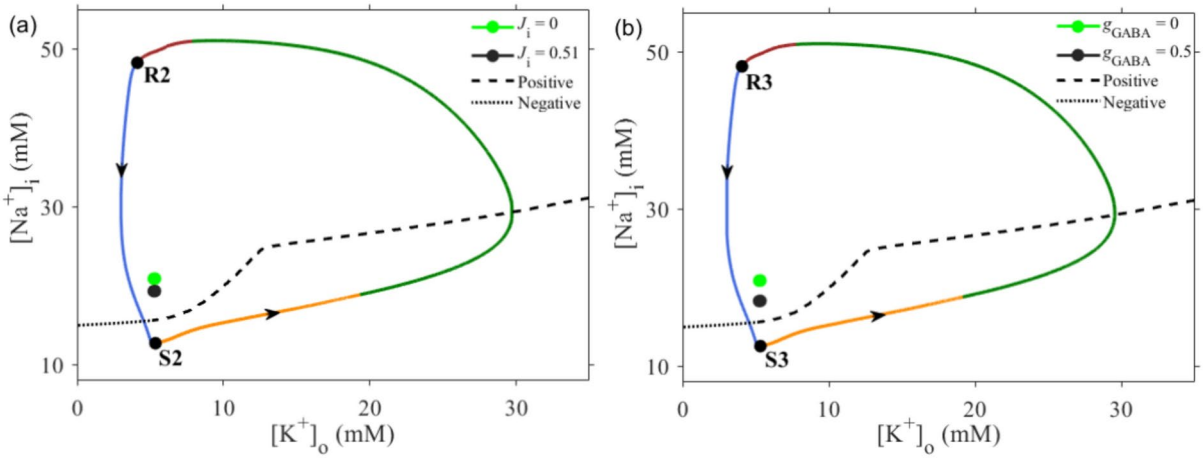

Fig. 8. Phase trajectory of uncommon MMB from coupling model runs across the "negative" threshold (dotted black curve). (**a**) The big cycle corresponds to the right solid circle in Fig. 6(a1). The silence phase is between R2 and S2; (**b**) The big cycle corresponds to the upper triangle in Fig. 6(a1). The silence phase is between R3 and S3.

respectively, locating upper to the "negative" threshold and corresponding to spiking when uncoupling. The spiking corresponding to the middle circle and middle triangle of Fig. 6(a1) is shown by the black circle in Fig. 8(a, b), respectively, locating upper to the "negative" threshold.

Uncommon MMB induces SD in a pyramidal neuronal network

A pyramidal neuronal network with square topology (51×51 neurons) and the lateral diffusion of K^+ is studied. Without loss of generality, a pyramidal neuron with location ($r = 14$ and $u = 27$) is randomly chosen as representative, which receives inhibitory synaptic current from interneuron, as shown by red triangle in Fig. 10 of Sect "Models and methods".

SD in the pyramidal neuronal networks

The uncommon MMB of neuron (14, 27) induces SD in the pyramidal neuronal network with τ_{diff} = 10 s, as shown in Fig. 9. In each panel, x and y coordinates mean the locations (r, u) of neurons. The white region

indicates the high $[K^+]_o$ for the depolarization block phase and small oscillation phase of the MMB, and black region for the burst phase and silence phase.

The interneuron for J_i = 1 μA and g_{GABA} = 1 mS/cm^2 exhibits low spiking frequency, which cannot induce uncommon MMB in the pyramidal neuron (14, 27). Then, not SD but stable spiking behavior with low $[K^+]_o$ (black) appears in the network, as shown in Fig. 9a (t = 0). For $t > 0$, J_i increases to 4 μA and g_{GABA} increases to 3 mS/cm^2, which can induce uncommon MMB in the pyramidal neuron (14, 27) around t = 152 s. Then, the depolarization block phase with high $[K^+]_o$ can evoke SD in the network via the lateral diffusion of $[K^+]_o$. Around the 158-th second (Fig. 9b), SD (white) is initiated by the depolarization block phase of the uncommon MMB of the neuron (14, 27), propagating to less than half of the neurons at the 175-th second (Fig. 9c), whereas the neurons surrounding the neuron (14, 27) exhibit recovery. Around the 180-th second (Fig. 9d), SD propagates to more than half of the neurons but the neurons surrounding (14, 27) recover to the initial spiking behavior. Around the 215-th second, all neurons recover to the spiking behaviors, resembling the panel (a) (not shown here).

For τ_{diff} = 5 s and 2 s, the results are similar, except that the initiation of SD is earlier and the propagation of SD is faster. The videos of the SD evoked by the interneuron for τ_{diff} = 10, 5, and 2 s are presented in Appendix A of the present paper. The first 120 s which shows only black panel with low $[K^+]_o$ for the spiking phase is ignored.

Membrane potential and extracellular potassium concentration of pyramidal neurons for SD

The membrane potential (left column) and $[K^+]_o$ (right column) are shown in the lower row of Fig. 9. From top to bottom, i.e., the subscript from 1 to 4, corresponds to the four pyramidal neurons marked by red dots from left to right in Fig. 9a–d. The uncommon MMB of the pyramidal neuron (14, 27) is depicted in Fig. 9(e1). The MMB of other neurons is induced by lateral diffusion of K^+, for instance, the pyramidal neurons (27,27) in Fig. 9(e2), (39,27) in Fig. 9(e3), and (51,27) in Fig. 9(e4). $[K^+]_o$ exhibits high value in the depolarization block phase, as depicted in Fig. 9(f1), (f2), (f3), and (f4). The vertical dashed lines denote the time shown in upper row of Fig. 9. The black arrows in the right panel show the propagation of the SD and $[K^+]_o$. The results for τ_{diff} = 5 s and 2 s are similar (not shown here).

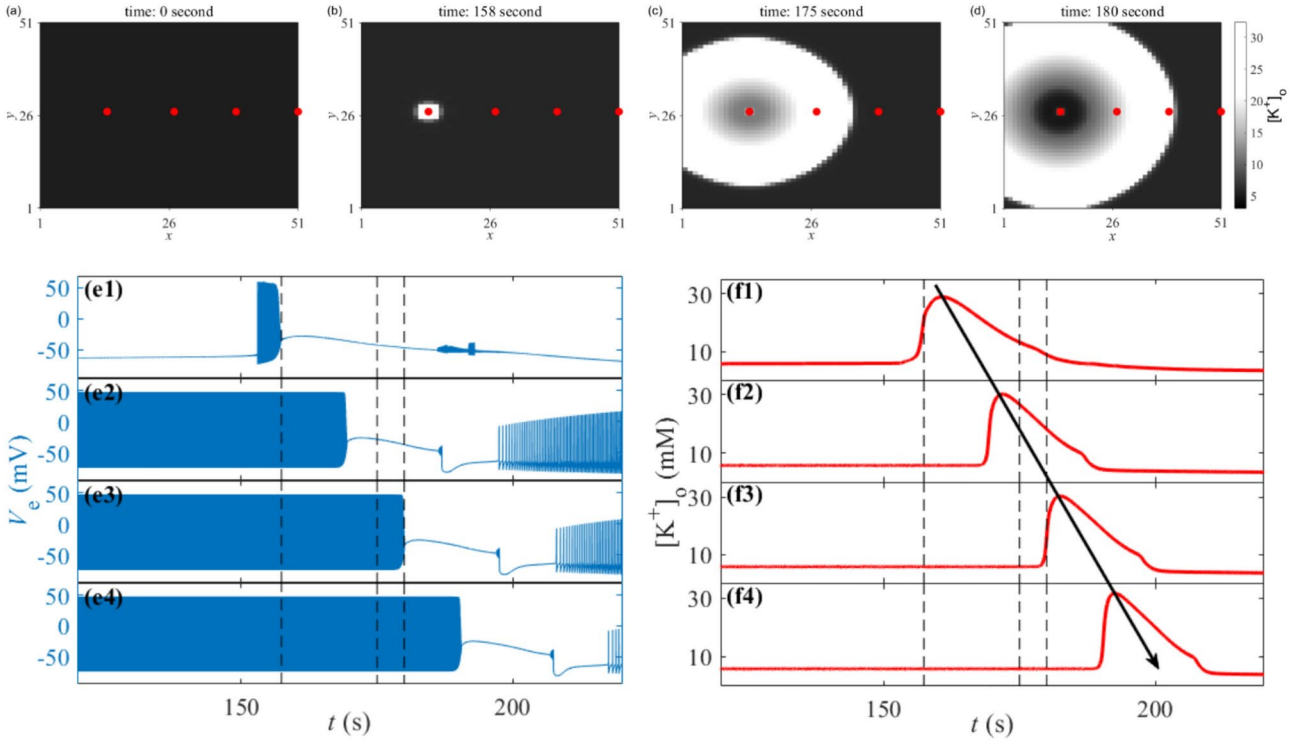

Fig. 9. SD induced by uncommon MMB in the pyramidal neuronal networks for τ_{diff} = 10 s. (**a**) t = 0 s; (**b**) t = 158 s; (**c**) t = 175 s; (**d**) t = 180 s. In each panel, the y-coordinates of all four red dots are 27, and x-coordinates are 14, 27, 39, and 51 from left to right. Lower row: the membrane potential (left column) and $[K^+]_o$ (right column) for the four pyramidal neurons labeled with red dots in the upper row. Panels (e1) and (f1) represent the uncommon MMB.

Conclusion and discussion

Recently, a counterintuitive phenomenon for the inhibitory interneuron, MMB in a single pyramidal neuron along with SD in the cerebral cortex, is observed in the experiments[21,22], presenting a novel etiology of FHM (type III) and a special case of seizure[36–41]. Inspired by a representative of counterintuitive phenomenon, the PIR phenomenon, which is explained with threshold and bifurcations[17–19], in the present paper, we present a novel mechanism for the MMB induced by inhibitory current and the SD induced by the uncommon MMB. The results exhibit significances in the following aspects:

Firstly, uncommon MMB is induced by the inhibitory current in a single neuron model and a coupling model, presenting a novel view on the MMB and a novel counterintuitive phenomenon of the inhibitory effect. Furthermore, the conditions of the pyramidal neuron, interneuron, and inhibitory synapse to induce and eliminate the uncommon MMB are acquired, presenting potential measures to modulate the MMB. The inhibitory neuron with high spiking frequency, the inhibitory synapse with large conductance, and the pyramidal neuron with high frequency, are favorable for the uncommon MMB. The inhibitory neuron with high spiking frequency resembles the experimental observations[21,22]. Then, changing the parameter of the inhibitory neuron to reduce the spiking frequency, such as reducing the sodium conductance, reducing the conductance of the inhibitory synapse, and reducing the spiking frequency of the pyramidal neuron, are the potential measures to eliminate the uncommon MMB. Among these measures, reducing the sodium conduction maybe the effective measure to suppress uncommon MMB for type III FHM with overexpression of sodium channel[21,22].

Secondly, the nonlinear mechanism and dynamical process for the uncommon MMB are obtained, presenting a deep understanding to the uncommon MMB. The pyramidal neuron with a high frequency spiking exhibits a biphasic threshold for the MMB, not only the well-known "positive" part, but also a novel "negative" part, like the PIR phenomenon[17–19]. The inhibitory stimulations with long duration and strong strength can induce the spiking of the pyramidal neuron changed to silence via the SNIC bifurcation at first, and then run across the "negative" threshold, triggering the positive feedback to form the depolarization block phase. Then, the SNIC bifurcation from spiking to silence, the "negative" part of the threshold, and the positive feedback ensure the formation of the uncommon MMB. The "negative" threshold is the most crucial cause for uncommon MMB. Different from the PIR phenomenon, the threshold of MMB is for $\left[K^+\right]_o$ instead of membrane potential.

Thirdly, the distinctions between the uncommon MMB and the common MMB induced by $\left[K^+\right]_o$ elevation (or excitatory effect) are obtained, which presents comprehensive view on the MMB. Different from the uncommon MMB which runs across the "negative" threshold, the common MMB runs across the "positive" threshold. The "negative" threshold has low $\left[K^+\right]_o$, whereas the "positive" threshold has high $\left[K^+\right]_o$. Then, in theory, uncommon and common MMB are different cases of MMB induced by different factors via different threshold mechanisms.

Finally, the SD induced by the uncommon MMB evoked by the enhanced activity of interneuron is reproduced in the pyramidal neuron network, presenting a novel mechanism for the SD and etiology of type III FHM and seizure. If no uncommon MMB is evoked in a pyramidal neuron, then, no SD is induced in the network.

Although the progresses of the present paper, the MMB and SD are influenced by multiple factors. In future, the inhibitory autapse which widely exists in the inhibitory neurons[42,43], the excitatory synapse from the pyramidal neuron to the inhibitory interneurons[24–26] ignored in the present paper, uptake of extracellular potassium ions by glial cells[44–46], should be considered to study their influences on the MMB and SD. Considering that the common MMB is induced by the release of K^+ of the interneuron[47,48], it may be more reasonable if both the inhibitory current and release of K^+ of the interneuron are considered to study the MMB for the type III FHM, which will be studied in future. Importantly, the competition and cooperation between the inhibitory current and release of K^+ should be investigated. In addition, more factors to modulate the network dynamics of SD, such as the excitatory synapses between pyramidal neurons, number of pyramidal neurons and interneurons, the topology of network, should be considered in future.

Models and methods

Coupling model of a pyramidal neuron and an interneuron

To focus on the inhibitory synaptic current, as shown in Fig. 10a, a pyramidal neuron receiving inhibitory synaptic current from an inhibitory interneuron for the coupling model, with the excitatory synapse from the pyramidal neuron to the interneuron ignored, since it can be speculated that the excitatory synapse can enhance activity of the interneuron. Then, the excitatory synapse may facilitate the uncommon MMB, which will be studied in future.

Pyramidal neuron model

A pyramidal neuron model used in Ref[24] is employed and described as follows:

$$C_{\rm me}\frac{{\rm d}V_{\rm e}}{{\rm d}t} = J_{\rm e} - (I_{\rm K} + I_{\rm Na} + I_{\rm L} + I_{\rm NaP} + I_{\rm AHP} + I_{\rm pump}) \tag{1}$$

$$\frac{{\rm d}n}{{\rm d}t} = a_n\,(1-n) - b_n n \tag{2}$$

$$\frac{{\rm d}h}{{\rm d}t} = a_h\,(1-h) - b_h h \tag{3}$$

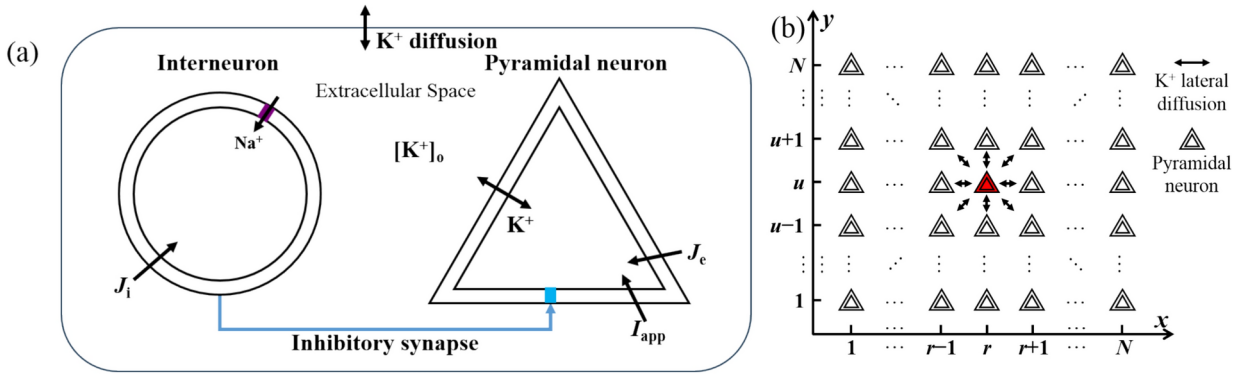

Fig. 10. Sketch map of the coupling model and the network model. (**a**) An inhibitory synapse (blue arrow) from the interneuron (left) to the pyramidal neuron (right). The over-expressed sodium (Na^+) channel is labeled, and J_i represent the depolarization current for interneuron. J_e represent the depolarization current and I_{app} denotes the negative pulse stimulation to the pyramidal neuron, and the black two-way arrows indicate the movement of potassium ions. $[K^+]_o$ stands for the extracellular potassium ion concentration; (**b**) Network composed of $N \times N$ pyramidal neurons with K^+ ion diffusion in the extracellular space between two adjacent neurons (lateral diffusion, two-way arrows). The red one (r, u) is suppressed by an inhibitory synapse from an interneuron.

$$\frac{d[Ca^{2+}]_i}{dt} = -\frac{\gamma}{2} g_{Ca} m_{\infty Ca} (V_e - E_{Ca}) - \frac{[Ca^{2+}]_i}{\tau_{Ca}} \tag{4}$$

$$\frac{d[K^+]_o}{dt} = \frac{1}{\tau} [\gamma\beta (I_K + I_{AHP} + I_{KL} - 2I_{pump}) + \beta (I_{KCC} + I_{NKCC}) - I_{diffKo}] \tag{5}$$

$$\frac{d[K^+]_i}{dt} = -\frac{1}{\tau} [\gamma (I_K + I_{AHP} + I_{KL} - 2I_{pump}) + (I_{KCC} + I_{NKCC}) + I_{diffKi}] \tag{6}$$

$$\frac{d[Na^+]_i}{dt} = \frac{1}{\tau} [-\gamma (I_{Na} + I_{NaP} + I_{NaL} + 3I_{pump}) - I_{NKCC}] \tag{7}$$

$$\frac{d[Cl^-]_i}{dt} = \frac{1}{\tau} (\gamma I_{ClL} - I_{KCC} - 2I_{NKCC}) \tag{8}$$

where V_e denotes the membrane voltage, n and h are the gating variables of K^+ channel and Na^+ channel, respectively. $[Ca^{2+}]_i$, $[K^+]_o$, $[K^+]_i$, $[Na^+]_i$, and $[Cl^-]_i$ denotes the concentrations of intracellular calcium, extracellular K^+, intracellular K^+, intracellular Na^+, and intracellular chloride (Cl^-), respectively. $[K^+]_o$, $[K^+]_i$, $[Na^+]_i$, and $[Cl^-]_i$ are four slow variables, since $\tau = 1000$ is very large. Then, fast-slow analysis to the MMB is difficult since multiple slow variables.

In Eq. (1), C_{me} is the membrane capacitance, and J_e means the depolarization current to enhance the firing activity. I_{Na} and I_K are the Na^+ and K^+ current, respectively. I_L represents the leak current, which is composed of sodium leak (I_{NaL}), potassium leak (I_{KL}), and chlorine leak (I_{ClL}) currents. I_{NaP}, I_{AHP}, and I_{pump} refer to the persistent sodium, calcium-activated potassium, and sodium–potassium pump currents, respectively. The detailed expressions of these currents in Eq. (1) are described as follows: $I_L = I_{NaL} + I_{KL} + I_{ClL}$, $I_{NaL} = g_{NaL}(V_e - E_{Na})$, $I_{KL} = g_{KL}(V_e - E_K)$, $I_{ClL} = g_{ClL}(V_e - E_{Cl})$, $I_K = g_K n^4 (V_e - E_K)$, $I_{Na} = g_{Na} m_{\infty Na}^3 h (V_e - E_{Na})$, $I_{NaP} = g_P m_{\infty Na}^3 (V_e - E_{Na})$, $I_{AHP} = g_{AHP} [Ca^{2+}]_i / ([Ca^{2+}]_i + 1)(V_e - E_K)$, $I_{pump} = \rho_{pump} / [1 + \exp(3.5 - [K^+]_o)] / [1 + \exp((22 - [Na^+]_i)/3)] / \gamma$, $m_{\infty Na} = a_m / (a_m + b_m)$, $a_m = 0.32(V_e + 54) / [1 - \exp(-(V_e + 54)/4)]$, $b_m = 0.28(V_e + 27) / [\exp((V_e + 27)/5) - 1]$, where g_{NaL}, g_{KL}, and g_{ClL} are the conductance. E_{Na}, E_K, and E_{Cl} denote the reversal voltage. g_K and g_{Na} represent the maximum conductance of I_K and I_{Na}, respectively, $m_{\infty Na}$ is steady state of activated variable. g_P, g_{AHP}, and ρ_{pump} denote the maximum conductance. $\gamma = S/(F \cdot Vol)$, where S and Vol denotes the surface and volume of the pyramidal neuron, and F is the Faraday constant.

In Eqs. (2), (3), n represents the activated gating variable of K^+ channel, and h denotes the inactivated gating variable of Na^+ channel. The functions in Eqs. (2), (3) are described as follows: $a_n = 0.032(V_e + 52) / [1 - \exp(-(V_e + 52)/5)]$, $b_n = 0.5\exp(-(V_e + 57)/40)$, $a_h = 0.128\exp(-(V_e + 50)/18)$, and $b_h = 4/[1 + \exp(-(V_e + 27)/5)]$.

In Eq. (4), g_{Ca} and $m_{\infty Ca}$ denote the maximum conductance and the steady state of activated variable of the calcium current $g_{Na}m_{\infty Na}(V_e - E_{Na})$, respectively, and $m_{\infty Na} = 1/[1 + \exp(-(V_e + 25)/2.5)]$. τ_{Ca} is the time constant of $[Ca^{2+}]_i$.

In Eqs. (5)–(8), I_{KCC} is K^+-Cl^- cotransporters and I_{NKCC} is Na^+-K^+-Cl^- cotransporters. I_{diffKo} and I_{diffKi} simulate the potassium diffusion in the extra- and intra-cellular space, respectively. The detailed expressions of the ion currents related to Eqs. (5)–(8) are described as follows: $I_{KCC} = 0.3\ln\left([K^+]_i[Cl^-]_i/\left([K^+]_o[Cl^-]_o\right)\right)$, $I_{NKCC} = 0.1\left[\ln\left([K^+]_i[Cl^-]_i/\left([K^+]_o[Cl^-]_o\right)\right) + \ln\left([Na^+]_i[Cl^-]_i/\left([Na^+]_o[Cl^-]_o\right)\right)\right]/\left[1 + \exp\left(16 - [K^+]_o\right)\right]$, $I_{diffKo} = \left([K^+]_o - K_{o0}\right)/\tau_{Ko}$, and $I_{diffKi} = \left([K^+]_i - K_{i0}\right)/\tau_{Ki}$, where τ_{Ko} and τ_{Ki} represent the time constant of extra- and intra-cellular K^+ diffusion, respectively, K_{o0} denotes the potassium concentration of the bathing solution. K_{i0} denotes the equilibrium concentration of intracellular K^+. $[Na^+]_o = 144\text{mM} - \beta\left([Na^+]_i - 18\text{mM}\right)$, $[Cl^-]_o = 130\text{mM} - \beta\left([Cl^-]_i - 6\text{mM}\right)$, where 144 mM and 18 mM is the sodium concentration outside and inside the neuron, respectively, and 130 mM and 6 mM correspond to the normal resting $[Cl^-]_o$ and $[Cl^-]_i$, respectively. The Nernst potentials of Na^+, K^+, and Cl^- are given as follows: $E_{Na} = 26.64\ln\left([Na^+]_o/[Na^+]_i\right)$, $E_K = 26.64\ln\left([K^+]_o/[K^+]_i\right)$, and $E_{Cl} = 26.64\ln\left([Cl^-]_i/[Cl^-]_o\right)$.

The parameter values of the pyramidal neuron are as follows: C_{me} = 1 μF/cm^2, g_{NaL} = 0.0015 mS/cm^2, g_{KL} = 0.05 mS/cm^2, g_{ClL} = 0.015 mS/cm^2, g_{Na} = 100 mS/cm^2, g_P = 1 mS/cm^2, g_K = 80 mS/cm^2, g_{AHP} = 1.5 mS/cm^2, E_{Ca} = 120 mV, g_{Ca} = 1 mS/cm^2, τ=1000,$\beta = 4$, τ_{Ca} = 80 ms, ρ_{pump} = 0.25 mM/s, τ_{Ko} = 2.5 s, K_{o0} = 3.5 mM, Vol=1.4368·10^{-9} cm^3, $S = 4\pi[3Vol/(4\pi)]^{2/3}$, τ_{Ki} = 250 s , and K_{i0} = 140 mM.

In the present paper, J_e to modulate the firing behavior is chosen as the control parameter. In addition, I_{app} to represent a negative square current is applied to Eq. (1), when the response of the pyramidal neuron to the inhibitory stimulation is studied.

Wang-Buzsaki model to describe the interneuron

The Wang-Buzsaki (WB) model in Ref[24] is used in the present paper and described as follows:

$$C_{mi}\frac{dV_i}{dt} = J_i - (I_{Ki} + I_{Nai} + I_{Li}) \tag{9}$$

$$\frac{dn_i}{dt} = 5\left[a_{ni}(1 - n_i) - b_{ni}n_i\right] \tag{10}$$

$$\frac{dh_i}{dt} = 5\left[a_{hi}(1 - h_i) - b_{hi}h_i\right] \tag{11}$$

where V_i denotes the membrane voltage, n_i is activated gating variable of the potassium current I_{Ki}, and h_i is inactivated gating variable of the sodium current I_{Nai}. In Eqs. (9)–(11), C_{mi} is the membrane capacitance, J_i is the depolarization current, and I_{Li} signifies the leak current. The detailed expressions of these currents are given as follows: $I_{Li} = g_{Li}(V_i - E_{Li})$, $I_{Ki} = g_{Ki}n_i^4(V_i - E_{Ki})$, and $I_{Nai} = g_{Nai}m_{\infty i}^3h_i(V_i - E_{Nai})$.

The equations related to the gating variables of the interneuron are as follows: $m_{\infty i} = a_{mi}/(a_{mi} + b_{mi})$, $a_{mi} = 0.1(V_i + 35)/[1 - \exp(-(V_i + 35)/10)]$, $b_{mi} = 4\exp(-(V_i + 60)/18)$, $a_{ni} = 0.01(V_i + 34)/[1 - \exp(-(V_i + 34)/10)]$, $b_{ni} = 0.125\exp(-(V_i + 44)/80)$, $a_{hi} = 0.07\exp(-(V_i + 58)/20)$, and $b_{hi} = 1/[1 + \exp(-(V_i + 28)/10)]$.

In the present paper, J_i and g_{Nai} to modulate the spiking rate are taken as the control parameters. Other parameter values are: C_{mi} = 1 μF/cm^2, g_{Li} = 0.1 mS/cm^2, g_{Ki} = 9 mS/cm^2, E_{Nai} = 55 mV, E_{Li} = −65 mV, and E_{Ki} = −90 mV.

Coupling neuronal model and synaptic model

Inhibitory current I_{GABA} is introduced to Eqs. (1), (8) to form Eqs. (12), (13) (other equations remain unchanged), respectively, which are described as follows:

$$C_{me}\frac{dV_e}{dt} = J_e - (I_K + I_{Na} + I_L + I_{NaP} + I_{AHP} + I_{pump}) + I_{GABA} \tag{12}$$

$$\frac{d[Cl^-]_i}{dt} = \frac{1}{\tau}\left[\gamma(I_{ClL} - I_{GABA}) - I_{KCC} - 2I_{NKCC}\right] \tag{13}$$

I_{GABA} modulates the electrical behavior of the membrane in Eq. (12) and $[Cl^-]_i$ in Eq. (13), since I_{GABA} is mediated by Cl^-. The equation for the I_{GABA} is as follows:

$$I_{GABA} = -g_{GABA}s(V_e - E_{Cl}) \tag{14}$$

where g_{GABA} is the synaptic conductance, E_{Cl} is the reversal potential, and s is the gating variable. In the present paper, s is set to 1 following a spike of the interneuron, and then obeys the following equation which is used in Ref[24]:

$$\frac{ds}{dt} = -\frac{s}{\tau_{GABA}} \tag{15}$$

with the synaptic time constant $\tau_{GABA} = 9$ ms.

Then, a 12-dimensional coupling model containing Eqs. (12), (13), Eqs. (2), (3), (4), (5), (6), (7), Eqs. (9), (10), (11), and Eq. (15) is obtained. In the present paper, g_{GABA} to control the inhibitory current is taken as the control parameter. The effect of the inhibitory current can be removed by setting $g_{GABA} = 0$ mS/cm^2.

Network model of the pyramidal neurons

In the present paper, $N \times N$ ($N = 51$) pyramidal neurons comprising a network with a square structure are considered. The lateral diffusion of potassium ion between neighboring neurons used in Refs[49–51] are considered as coupling. The two-dimensional pyramidal neuronal network is formulated as follows:

$$C_{me}\frac{dV_e^{r,u}}{dt} = J_e - \left(I_K^{r,u} + I_{Na}^{r,u} + I_L^{r,u} + I_{NaP}^{r,u} + I_{AHP}^{r,u} + I_{pump}^{r,u}\right) \tag{16}$$

$$\frac{dn^{r,u}}{dt} = a_n^{r,u}\left(1 - n^{r,u}\right) - b_n^{r,u}n^{r,u} \tag{17}$$

$$\frac{dh^{r,u}}{dt} = a_h^{r,u}\left(1 - h^{r,u}\right) - b_h^{r,u}h^{r,u} \tag{18}$$

$$\frac{d\left[Ca^{2+}\right]_i^{r,u}}{dt} = -\frac{\gamma}{2}g_{Ca}m_{\infty Ca}^{r,u}\left(V_e^{r,u} - E_{Ca}^{r,u}\right) - \frac{\left[Ca^{2+}\right]_i^{r,u}}{\tau_{Ca}} \tag{19}$$

$$\frac{d\left[K^+\right]_o^{r,u}}{dt} = \frac{1}{\tau}\left[\gamma\beta\left(I_K^{r,u} + I_{AHP}^{r,u} + I_{KL}^{r,u} - 2I_{pump}^{r,u}\right) + \beta\left(I_{KCC}^{r,u} + I_{NKCC}^{r,u}\right) - I_{diffKo}^{r,u} + I_{diff}^{r,u}\right] \tag{20}$$

$$\frac{d\left[K^+\right]_i^{r,u}}{dt} = -\frac{1}{\tau}\left[\gamma\left(I_K^{r,u} + I_{AHP}^{r,u} + I_{KL}^{r,u} - 2I_{pump}^{r,u}\right) + \left(I_{KCC}^{r,u} + I_{NKCC}^{r,u}\right) + I_{diffKi}^{r,u}\right] \tag{21}$$

$$\frac{d\left[Na^+\right]_i^{r,u}}{dt} = \frac{1}{\tau}\left[-\gamma\left(I_{Na}^{r,u} + I_{NaP}^{r,u} + I_{NaL}^{r,u} + 3I_{pump}^{r,u}\right) - I_{NKCC}^{r,u}\right] \tag{22}$$

$$\frac{d\left[Cl^-\right]_i^{r,u}}{dt} = \frac{1}{\tau}\left(\gamma I_{ClL}^{r,u} - I_{KCC}^{r,u} - 2I_{NKCC}^{r,u}\right) \tag{23}$$

where the superscripts r and u represent the coordinates x and y of a neuron in the network. The lateral diffusion between neuron (r, u) and its neighboring neurons (z, w) in Eq. (20) is described as follows:

$$I_{diff}^{r,u} = \sum_{z,w}\frac{1}{\tau_{diff}}\varepsilon^{r,u,z,w}\left(\left[K^+\right]_o^{z,w} - \left[K^+\right]_o^{r,u}\right) \tag{24}$$

where τ_{diff} represents the time constant of the lateral diffusion. If the neuron (r, u) is one of the four corners of the network, it is coupled to three neighboring neurons. If the neuron (r, u) is one on the four borders exclusive the corners of the network, it is coupled to five neighboring neurons. If the neuron (r, u) is not located on the borders of the network, it is coupled to eight neighboring neurons. Then, $\varepsilon^{r,u,z,w} = 1$ for the neighboring neurons and $\varepsilon^{r,u,z,w} = 0$ for the remaining neurons. Except for $I_{diff}^{r,u}$, all parameters and functions of neurons in the network are the same as the isolated neurons, with $J_e = 4$ μA. The pyramidal neurons in the network exhibit spiking when isolated. The time constant τ_{diff} is regarded as control parameter.

Without loss of generality, a pyramidal neuron ($r = 14$, $u = 27$) is randomly chosen as representative, which receives an inhibitory synaptic current from an inhibitory interneuron. As the inhibitory neuron exhibits enhanced activity to induce uncommon MMB in the pyramidal neuron (14, 27), the propagation of the depolarization block phase of the uncommon MMB to other neurons to form the SD in the network is studied. In the present paper, we mainly show that the uncommon MMB evoked in a pyramidal neuron can propagate in the pyramidal neuronal networks to form the SD, which are mainly influenced by the lateral diffusion of extracellular potassium ions here. In the real system, the network dynamics of SD are influenced by more factors, such as the excitatory synapses between pyramidal neurons, number of pyramidal neurons and interneurons, the topology of network composed of the pyramidal neurons and interneurons, which will be studied in future.

Calculation of the threshold for the MMB of the pyramidal neuron

The threshold for an action potential is a well-known nonlinear concept to characterize the response of a neuron to external stimulations. The threshold is an intrinsic characteristic to identify the dynamics evolving from different initial values, which can also be used to identify the dynamics induced by external stimulations, which can induce changes of the initial values. For example, there is a positive threshold for the general action potential induced from resting state by positive stimulation, and a negative threshold for the PIR spike evoked from the resting state by inhibitory stimulation[17–20]. The membrane potential for the positive threshold is higher than that of the resting state, and for the negative threshold is lower than that of the resting state. The relationship between

the "positive" threshold, "negative" threshold, and resting state is used as reference to understand the threshold of $[K^+]_o$ for the MMB.

In the present paper, we calculate the threshold for the MMB of the pyramidal neuron induced from a spiking behavior by $[K^+]_o$ or the inhibitory stimulations. For the equations of a neuron model at spiking behavior, an external stimulation induces the change of the variable values. At the termination time of the stimulation, the values of the variables can be regarded as the novel initial values of the model. The behaviors beginning from the novel initial values result in two behaviors, which are dependent of the stimulation. One is the MMB at first and then recovers to spiking, called suprathreshold, and the other is still spiking, called subthreshold. Then, the suprathreshold and subthreshold for the initial values in a wide range of phase space are calculated. The border between the initial values for the suprathreshold and subthreshold forms the threshold. The initial values for the suprathreshold and subthreshold comprise the MMB region and spiking region, respectively.

In the present paper, the pyramidal neuron model is eight-dimenional, then, the threshold is 8-dimensional. Projection of the threshold in two-dimensional plane or three-dimensional space, which can be visualized, is presented. $[K^+]_o$ is one variable of the projection plane or space, since the key dynamics for the MMB is that $[K^+]_o$ exhibits nearly "all-or-none" characteristic (similar to the action potential) and $[K^+]_o$ is the most important factor which has been related to the MMB[21,22,24–26]. Then, the threshold for $[K^+]_o$ is mainly studied in the present paper, although other variables such as $[Na^+]_i$ also exhibit threshold. If the threshold for $[K^+]_o$ exhibits a part locating "negative" to that of the spiking, i.e., "negative" threshold, the uncommon MMB should be induced by negative stimulation. $[K^+]_o$ decreases at first and then runs across the "negative" threshold. If the threshold for $[K^+]_o$ manifests a part locates "positive" to the spiking, i.e., "positive" threshold, the excitatory stimulation or enhancement of $[K^+]_o$ can induce the MMB. $[K^+]_o$ increases at first and then passes through the "positive" threshold. Then, the threshold is used to identify the dynamics induced by $[K^+]_o$ pulse stimulation (Fig. 2c, d in the present paper), negative pulse stimulation (Fig. 3a, b), and negative synaptic current (Fig. 8). If the stimulation can induce spiking of pyramidal neuron run across the threshold, MMB is induced. If not, still spiking instead of MMB is induced.

Methods

The bifurcations of single pyramidal neuron are obtained using the available software XPPAUT[52]. The numerical solutions of single neuron, coupling model, and neuronal networks are solved using the fourth order Runge–Kutta method with a time step 0.001 ms.

Data availability

The datasets generated during and/or analyzed during the current study are available from the corresponding author on reasonable request.

Received: 28 November 2024; Accepted: 3 March 2025
Published online: 14 March 2025

References

1. O'Hare, L., Tarasi, L., Asher, J. M., Hibbard, P. B. & Romei, V. Excitation-inhibition imbalance in migraine: from neurotransmitters to brain oscillations. *Int. J. Mol. Sci.* **24**(12), 10093. https://doi.org/10.3390/ijms241210093 (2023).
2. van Hugte, E. J. H., Schubert, D. & Nadif, K. N. Excitatory/inhibitory balance in epilepsies and neurodevelopmental disorders: Depolarizing γ-aminobutyric acid as a common mechanism. *Epilepsia* **64**(8), 1975–1990. https://doi.org/10.1111/epi.17651 (2023).
3. Liu, Y., Grigorovsky, V. & Bardakjian, B. Excitation and inhibition balance underlying epileptiform activity. *IEEE Trans. Biomed. Eng.* **67**(9), 2473–2481. https://doi.org/10.1109/TBME.2019.2963430 (2020).
4. Naylor, D. E., Liu, H. & Wasterlain, C. G. Trafficking of GABA(A) receptors, loss of inhibition, and a mechanism for pharmacoresistance in status epilepticus. *J. Neurosci.* **25**(34), 7724–7733. https://doi.org/10.1523/JNEUROSCI.4944-04.2005 (2005).
5. Bragin, A., Azizyan, A., Almajano, J. & Engel, J. The cause of the imbalance in the neuronal network leading to seizure activity can be predicted by the electrographic pattern of the seizure onset. *J. Neurosci.* **29**, 3660–3671. https://doi.org/10.1523/JNEUROSCI.5309-08 (2009).
6. Mermer, F. et al. Astrocytic GABA transporter 1 deficit in novel SLC6A1 variants mediated epilepsy: Connected from protein destabilization to seizures in mice and humans. *Neurobiol. Dis.* **172**, 105810. https://doi.org/10.1016/j.nbd.2022.105810 (2022).
7. Liddiard, G. T., Suryavanshi, P. S. & Glykys, J. Enhancing GABAergic tonic inhibition reduces seizure-like activity in the neonatal mouse hippocampus and neocortex. *J. Neurosci.* **44**(7), e1342232023. https://doi.org/10.1523/JNEUROSCI.1342-23.2023 (2024).
8. Krook-Magnuson, E., Armstrong, C., Oijala, M. & Soltesz, I. On-demand optogenetic control of spontaneous seizures in temporal lobe epilepsy. *Nat. Commun.* **4**, 1376. https://doi.org/10.1038/ncomms2376 (2013).
9. Greenfield, L. J. Molecular mechanisms of antiseizure drug activity at GABAA receptors. *Seizure* **22**(8), 589–600. https://doi.org/10.1016/j.seizure.2013.04.015 (2013).
10. Borges, F. S. et al. Intermittency properties in a temporal lobe epilepsy model. *Epilepsy Behav.* **139**, 109072. https://doi.org/10.1016/j.yebeh.2022.109072 (2023).
11. Ben-Ari, Y., Gaiarsa, J. L., Tyzio, R. & Khazipov, R. GABA: a pioneer transmitter that excites immature neurons and generates primitive oscillations. *Physiol. Rev.* **87**(4), 1215–1284. https://doi.org/10.1152/physrev.00017.2006 (2007).
12. Gulledge, A. T. & Stuart, G. J. Excitatory actions of GABA in the cortex. *Neuron* **37**(2), 299–309. https://doi.org/10.1016/s0896-6273(02)01146-7 (2003).
13. Elahian, B. et al. Low-voltage fast seizures in humans begin with increased interneuron firing. *Ann. Neurol.* **84**(4), 588–600. https://doi.org/10.1002/ana.25325 (2018).
14. Sessolo, M. et al. Parvalbumin-positive inhibitory interneurons oppose propagation but favor generation of focal epileptiform activity. *J. Neurosci.* **35**(26), 9544–9557. https://doi.org/10.1523/JNEUROSCI.5117-14.2015 (2015).
15. Assaf, F. & Schiller, Y. The antiepileptic and ictogenic effects of optogenetic neurostimulation of PV-expressing interneurons. *J. Neurophysiol.* **116**(4), 1694–1704. https://doi.org/10.1152/jn.00744.2015 (2016).
16. Chang, M. et al. Brief activation of GABAergic interneurons initiates the transition to ictal events through post-inhibitory rebound excitation. *Neurobiol. Dis.* **109**(Pt A), 102–116. https://doi.org/10.1016/j.nbd.2017.10.007 (2018).

17. Izhikevich, E. M. Neural excitability, spiking and bursting. *Int. J. Bifurc. Chaos* **10**(6), 1171–1266. https://doi.org/10.1142/S0218127400000840 (2000).
18. Wang, X., Gu, H., Jia, Y., Lu, B. & Zhou, H. Bifurcations for counterintuitive post-inhibitory rebound spike related to absence epilepsy and Parkinson disease. *Chin. Phys. B* **32**, 090502. https://doi.org/10.1088/1674-1056/acd7d3 (2023).
19. Guan, L., Jia, B. & Gu, H. A novel threshold across which the negative stimulation evokes action potential near a saddle-node bifurcation in a neuronal model with Ih current. *Int. J. Bifurc. Chaos* **29**(14), 1950198. https://doi.org/10.1142/S0218127419501980 (2019).
20. Ma, K., Gu, H. & Jia, Y. The neuronal and synaptic dynamics underlying post-inhibitory rebound burst related to major depressive disorder in the lateral habenula neuron model. *Cogn. Neurodyn.* **18**(3), 1397–1416. https://doi.org/10.1007/s11571-023-09960-0 (2024).
21. Chever, O. et al. Initiation of migraine-related cortical spreading depolarization by hyperactivity of GABAergic neurons and NaV1.1 channels. *J. Clin. Investig.* **131**(21), e142203. https://doi.org/10.1172/JCI142203 (2021).
22. Auffenberg, E. et al. Hyperexcitable interneurons trigger cortical spreading depression in an Scn1a migraine model. *J. Clin. Investig.* **131**(21), e142202. https://doi.org/10.1172/JCI142202 (2021).
23. Călin, A., Ilie, A. S. & Akerman, C. J. Disrupting epileptiform activity by preventing parvalbumin interneuron depolarization block. *J. Neurosci.* **41**(45), 9452–9465. https://doi.org/10.1523/JNEUROSCI.1002-20.2021 (2021).
24. Desroches, M., Faugeras, O., Krupa, M. & Mantegazza, M. Modeling cortical spreading depression induced by the hyperactivity of interneurons. *J. Comput. Neurosci.* **47**(2–3), 125–140. https://doi.org/10.1007/s10827-019-00730-8 (2019).
25. Lemaire, L. et al. Modeling NaV1.1/SCN1A sodium channel mutations in a microcircuit with realistic ion concentration dynamics suggests differential GABAergic mechanisms leading to hyperexcitability in epilepsy and hemiplegic migraine. *PLoS Comput. Biol.* **17**(7), e1009239. https://doi.org/10.1371/journal.pcbi.1009239 (2021).
26. Stein, W. & Harris, A. L. Interneuronal dynamics facilitate the initiation of spike block in cortical microcircuits. *J. Comput. Neurosci.* **50**, 275–298. https://doi.org/10.1007/s10827-022-00815-x (2022).
27. Dichgans, M. et al. Mutation in the neuronal voltage-gated sodium channel SCN1A in familial hemiplegic migraine. *Lancet* **366**(9483), 371–377. https://doi.org/10.1016/S0140-6736(05)66786-4 (2005).
28. Bertelli, S., Barbieri, R., Pusch, M. & Gavazzo, P. Gain of function of sporadic/familial hemiplegic migraine-causing SCN1A mutations: use of an optimized cDNA. *Cephalalgia* **39**(4), 477–488. https://doi.org/10.1177/0333102418788336 (2019).
29. Li, D. et al. The role of extracellular glutamate homeostasis dysregulated by astrocyte in epileptic discharges: a model evidence. *Cogn. Neurodyn.* **18**(2), 485–502. https://doi.org/10.1007/s11571-023-10001-z (2024).
30. Contreras, S. A., Schleimer, J. H., Gulledge, A. T. & Schreiber, S. Activity-mediated accumulation of potassium induces a switch in firing pattern and neuronal excitability type. *PLoS Comput. Biol.* **17**(5), e1008510. https://doi.org/10.1371/journal.pcbi.1008510 (2021).
31. Cressman, J. R. J., Ullah, G., Ziburkus, J., Schiff, S. J. & Barreto, E. The influence of sodium and potassium dynamics on excitability, seizures, and the stability of persistent states: I. Single neuron dynamics. *J. Comput. Neurosci.* **26**(2), 159–170. https://doi.org/10.1007/s10827-008-0132-4 (2009).
32. de Curtis, M., Uva, L., Gnatkovsky, V. & Librizzi, L. Potassium dynamics and seizures: Why is potassium ictogenic?. *Epilepsy Res.* **143**, 50–59. https://doi.org/10.1016/j.eplepsyres.2018.04.005 (2018).
33. Chesebro, A. G., Mujica-Parodi, L. R. & Weistuch, C. Ion gradient-driven bifurcations of a multi-scale neuronal model. *Chaos Solitons Fractals* **167**, 113120. https://doi.org/10.1016/j.chaos.2023.113120 (2023).
34. Dumont, T. et al. Simulation of human ischemic stroke in realistic 3D geometry. *Commun. Nonlinear Sci. Numer. Simul.* **18**(6), 1539–1557. https://doi.org/10.1016/j.cnsns.2012.10.002 (2013).
35. Yu, Y., Yuan, Z., Li, J. & Wu, Y. Dynamic analysis of epileptic seizures caused by energy failure after ischemic stroke. *Chaos Solitons Fractals* **176**, 114116. https://doi.org/10.1016/j.chaos.2023.114116 (2023).
36. Fujiwara-Tsukamoto, Y. et al. Prototypic seizure activity driven by mature hippocampal fast-spiking interneurons. *J. Neurosci.* **30**(41), 13679–13689. https://doi.org/10.1523/JNEUROSCI.1523-10.2010 (2010).
37. Rich, S. et al. Inhibitory network bistability explains increased interneuronal activity prior to seizure onset. *Front. Neural Circuits* **13**, 81. https://doi.org/10.3389/fncir.2019.00081 (2020).
38. Liu, Z., De Schutter, E. & Li, Y. GABA-induced seizure-like events caused by multi-ionic interactive dynamics. *eNeuro* https://doi.org/10.1523/ENEURO.0308-24.2024 (2024).
39. Lin, C. H. et al. Effects of anti-epileptic drugs on spreading depolarization-induced epileptiform activity in mouse hippocampal slices. *Sci. Rep.* **7**(1), 11884. https://doi.org/10.1038/s41598-017-12346-y (2017).
40. Ziburkus, J., Cressman, J. R., Barreto, E. & Schiff, S. J. Interneuron and pyramidal cell interplay during in vitro seizure-like events. *J. Neurophysiol.* **95**(6), 3948–3954. https://doi.org/10.1152/jn.01378.2005 (2006).
41. Marcuccilli, C. J. et al. Neuronal bursting properties in focal and parafocal regions in pediatric neocortical epilepsy stratified by histology. *J. Clin. Neurophysiol.* **27**(6), 387–397. https://doi.org/10.1097/WNP.0b013e3181fe06d8 (2010).
42. Yin, L. et al. Autapses enhance bursting and coincidence detection in neocortical pyramidal cells. *Nat. Commun.* **9**(1), 4890. https://doi.org/10.1038/s41467-018-07317-4 (2018).
43. Bacci, A. & Huguenard, J. R. Enhancement of spike-timing precision by autaptic transmission in neocortical inhibitory interneurons. *Neuron* **49**(1), 119–130. https://doi.org/10.1016/j.neuron.2005.12.014 (2006).
44. Florence, G., Pereira, T. & Kurths, J. Extracellular potassium dynamics in the hyperexcitable state of the neuronal ictal activity. *Commun. Nonlinear Sci. Numer. Simul.* **17**(12), 4700–4706. https://doi.org/10.1016/j.cnsns.2011.06.023 (2012).
45. Wei, Y., Ullah, G. & Schiff, S. J. Unification of neuronal spikes, seizures, and spreading depression. *J. Neurosci.* **34**(35), 11733–11743. https://doi.org/10.1523/JNEUROSCI.0516-14.2014 (2014).
46. Tagluk, M. E. & Tekin, R. The influence of ion concentrations on the dynamic behavior of the Hodgkin-Huxley model-based cortical network. *Cogn. Neurodyn.* **8**(4), 287–298. https://doi.org/10.1007/s11571-014-9281-5 (2014).
47. Wu, X. X. & Shuai, J. W. Multistability in a neuron model with extracellular potassium dynamics. *Phys. Rev. E Stat. Nonlinear Soft Matter Phys.* **85**(6), 61911. https://doi.org/10.1103/PhysRevE.85.061911 (2012).
48. Wu, X. X. & Shuai, J. Effects of extracellular potassium diffusion on electrically coupled neuron networks. *Phys. Rev. E Stat. Nonlinear Soft Matter Phys.* **91**(2), 22712. https://doi.org/10.1103/PhysRevE.91.022712 (2015).
49. Florence, G., Dahlem, M. A., Almeida, A. C., Bassani, J. W. & Kurths, J. The role of extracellular potassium dynamics in the different stages of ictal bursting and spreading depression: a computational study. *J. Theor. Biol.* **258**(2), 219–228. https://doi.org/10.1016/j.jtbi.2009.01.032 (2009).
50. Durand, D. M., Park, E. H. & Jensen, A. L. Potassium diffusive coupling in neural networks. *Philos. Trans. R. Soc. Lond. B Biol. Sci.* **365**(1551), 2347–2362. https://doi.org/10.1098/rstb.2010.0050 (2010).
51. Ullah, G., Cressman, J. R. J., Barreto, E. & Schiff, S. J. The influence of sodium and potassium dynamics on excitability, seizures, and the stability of persistent states II. Network and glial dynamics. *J. Comput. Neurosci.* **26**(2), 171–183. https://doi.org/10.1007/s10827-008-0130-6 (2009).
52. Ermentrout, B. Simulating, analyzing, and animating dynamical systems. In *A Guide to XPPAUT for Researchers and Students* (ed. Kani, B.) (SIAM Press, 2002).

Acknowledgements
This work was supported by the National Natural Science Foundation of China (Grant Nos. 12072236, 12372063, and 11802086)

Author contributions
H.H. and G.H. wrote the main manuscript text and prepared all the figures. All authors reviewed the manuscript. The details of each author's contribution to this work are as follows: H. H.: investigation, methodology, resources, software, validation, visualization, writing – original draft, writing – review & editing. G. H.: conceptualization, funding acquisition, investigation, methodology, resources, software, supervision, validation, visualization, writing – original draft, writing – review & editing. M. K.: investigation, methodology, software, visualization, writing – review & editing. J. Y.: funding acquisition, investigation, visualization, writing – review & editing. W. L.: software, visualization, writing – review & editing.

Declarations

Competing interests
The authors declare no competing interests.

Additional information
Supplementary Information The online version contains supplementary material available at https://doi.org/10.1038/s41598-025-92647-9.

Correspondence and requests for materials should be addressed to H.G.

Reprints and permissions information is available at www.nature.com/reprints.

Publisher's note Springer Nature remains neutral with regard to jurisdictional claims in published maps and institutional affiliations.